Copyright ©1997, American Institute of Aeronautics and Astronautics, Inc.

AIAA Meeting Papers on Disc, January 1997
A9715262, AIAA Paper 97-0179

Experimental determination of the droplet impingement characteristics of a propeller

Jonathan Reichhold
Illinois Univ., Urbana

Michael Bragg
Illinois Univ., Urbana

Dave Sweet
BFGoodrich Aerospace, Uniontown, OH

AIAA, Aerospace Sciences Meeting & Exhibit, 35th, Reno, NV, Jan. 6-9, 1997

One of the most powerful tools in the analysis of aircraft icing is the knowledge of where the water in a given cloud will impinge on a surface. The determination of where a structure will accrete ice is expressed by the impingement efficiency, beta. An improvement to the dye-tracer method for the experimental determination of impingement efficiency is presented. The improved method, which saves both time and expense, was then used to determine the impingement efficiency on a four-bladed, constant chord propeller with a nacelle. The propeller impingement tests showed the limitations of the current droplet impingement test techniques and found impingement efficiencies greater than one for a large portion of the propeller blade. Using blade-element theory it is shown how impingement efficiencies greater than one can occur for the case of a propeller. Suggestions are also made as to how the dye-tracer test method can be improved. (Author)

Copyright ©1997, American Institute of Aeronautics and Astronautics, Inc.

Experimental Determination of the Droplet Impingement Characteristics of a Propeller

Jonathan Reichhold* and Michael Bragg†
University of Illinois at Urbana/Champaign
Urbana, Illinois

Dave Sweet‡
BFGoodrich Aerospace - Deicing Systems
Uniontown, Ohio

ABSTRACT

One of the most powerful tools in an analysis of aircraft icing is the knowledge of where the water in a given cloud will impinge on an surface. The determination of where a structure will accrete ice is expressed by the impingement efficiency, β. An improvement to the dye-tracer method for the experimental determination of impingement efficiency is presented. The improved method, which saves both time and expense, was then used to determine the impingement efficiency on a four-bladed, constant chord propeller with a nacelle. The propeller impingement tests showed the limitations of the current droplet impingement test techniques and found impingement efficiencies greater than one for a large portion of the propeller blade. Using blade-element theory it is shown how impingement efficiencies greater than one can occur for the case of a propeller. Suggestions are also made as to how the dye-tracer test method can be improved.

INTRODUCTION

The design of aircraft for safe operation in icing environments requires a knowledge of where the water in an icing cloud will impinge. This information is necessary for the efficient design of the aircraft ice protection systems. Knowing the extent and mass of the impinging water, along with the flight and cloud conditions, determines the energy per unit area which must be supplied and the surfaces locations which must be protected.

Droplet impingement information is also a fundamental input in the prediction of the ice accretions which form on aircraft. The early methods to compute ice growth used a knowledge of the droplet impingement information to approximate the ice which formed on structures. More recent computational models utilize droplet impingement information directly in a time stepped manner to compute the formation of ice over time on a structure. These newer computational methods have evolved into highly specialized tools allowing the prediction of ice formations in aircraft development programs. Knowledge of the ice formations allows for the determination of the effects icing will have on the aerodynamics of a structure. The aerodynamics of the resultant structure with ice are important for the evaluation of aircraft safety margins.

The determination of droplet impingement information is most often accomplished by means of computational codes. These computational methods determine the mass of water which will impinge on a surface by the numerical solution of water droplet trajectories. While these codes do provide an efficient means to compute the droplet trajectories for a large number of structures, all computational methods require verification. These computational tools have been verified using the dye-tracer technique.

The dye-tracer method of droplet impingement was developed by von Glahn, et al.[1], in the 1950s. The dye-tracer method is based upon the injection of a known concentration of dyed water into a wind tunnel by means of spray nozzles to create a 'cloud' of water. The dye laden water contained in the resultant spray cloud was then allowed to impinge on a model which had been covered with an absorbent medium. The absorbent medium, typically a blotter paper strip, absorbed the dye in the spray cloud at the point of droplet impact. In a similar manner, a freestream reference collector was mounted in the test section to determine the mass flux of water at specified locations in the freestream over given spray times.

The mass of dye deposited at each location on the absorbent mediums, from the model and freestream,

* Formerly Graduate Research Assistant, Dept. of Aeronautical & Astronautical Engineering. Currently Engineer at The Boeing Company, Seattle, WA. Member AIAA
† Professor, Dept. of Aeronautical and Astronautical Engineering, Associate Fellow AIAA
‡ Manager of Research and Development
Copyright © 1997 by J. D. Reichhold and M. B. Bragg. Published by the American Institute of Aeronautics and Astronautics, Inc. with permission.

Copyright ©1997, American Institute of Aeronautics and Astronautics, Inc.

was directly proportional to the mass of water which impinged on the model at the corresponding location. After the dye was allowed to impinge on the model for a given time, the absorbent material was removed and reduced by means of a colorimetric analysis to determine the mass of dye which had impinged at several discrete locations on the paper.

In the NACA tests of von Glahn, dye extraction was accomplished by punching holes out of the data strips. The cut outs were then dissolved in a aqueous solution to separate the dye from the paper medium. Next, the paper strands remaining in the mixture were filtered out. The remaining dye and water solution was then analyzed with a colorimeter to determine the concentration of dye in the solution. From the dye concentration, knowing the amount of water used to extract the dye from the paper, the mass of dye in the solution was therefore determined.

A modified means of reducing the mass of dye from the paper strips was developed by Papadakis, et al.[2], in the late 1980s. Papadakis replaced the colorimetric analysis, which had been expensive, time consuming, and destructive, with a laser reflectance method. Instead of punching holes from the data strips, the laser reflectance data reduction used the reflected laser intensity from the data strip to determine the mass of dye in the paper itself. This method of data reduction was based upon diffuse reflective spectroscopy which states that the intensity of the reflected light was proportional to the mass of dye in the paper.

In 1995 Bragg, et al.[3], further improved the dye extraction method by using a digital camera to create an image of the dye laden strips. The digital image was then reduced by means of image analysis routines. This newer method provided a much faster and less expensive means to reduce the data strips. The theory and implementation of this method will be discussed briefly and are covered in further detail by Reichhold[4].

THEORY AND IMPLEMENTATION

The study of icing frequently requires the determination of droplet impingement parameters. The most frequently used droplet impingement parameters are the impingement efficiency, β, and the collection efficiency, E. The impingement efficiency is the mass flux of water impinging on a surface non-dimensionalized by the freestream mass flux. After utilizing conservation of mass the resultant equation for β is given by Eq. 1. Note that Fig. 1 illustrates the variables in the context of the propeller. The collection efficiency is the total mass flux impinging on a body non-dimensionalized by the mass flux in the freestream through a characteristic area. In practice the collection efficiency is defined as the integral of the impingement efficiency from the maximum upper surface impingement location, s_U, to the minimum lower surface impingement location, s_L, Eq. 2.

$$\beta = {A_f}/{A_o} \tag{1}$$

$$E = \frac{1}{A_{ref}} \int_{s_L}^{s_U} \beta \cdot dA \tag{2}$$

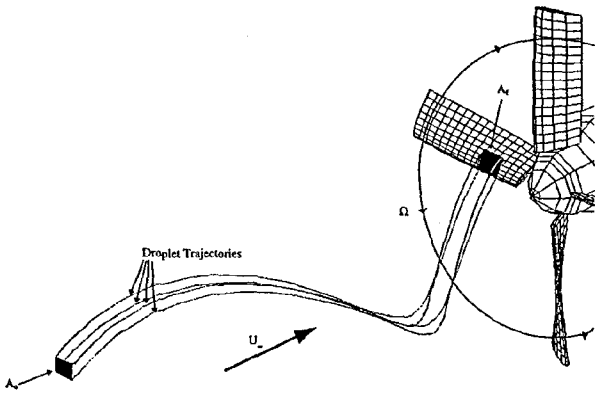

Fig. 1 Droplet trajectory parameters in 3-D

Dye Tracer Impingement Tests

The goal of the present study was to determine the impingement efficiency about a three-dimensional, rotating propeller. In order to accomplish this task, the UIUC 3-D tunnel, Fig. 2, was modified to include a spray system and propeller test stand. The UIUC tunnel had a maximum test section velocity of 45 ft/sec (with propeller and spray system installed) and used a spray system composed of five NASA standard spray nozzles. The spray system used the hardware from the tests of

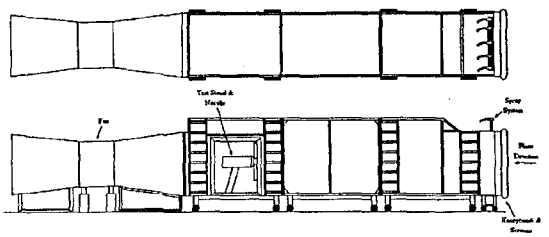

Fig. 2. UIUC 3-D tunnel setup.

Copyright ©1997, American Institute of Aeronautics and Astronautics, Inc.

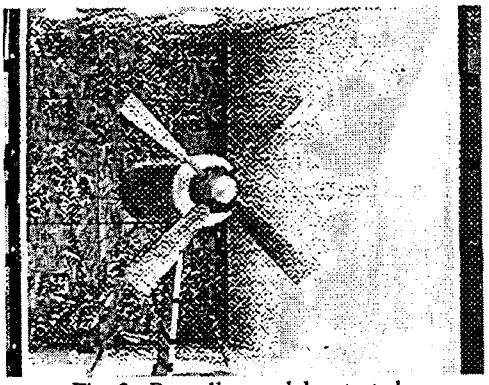

Fig. 3. Propeller model as tested.

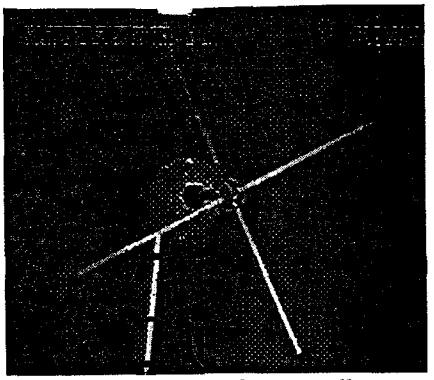

Fig. 4. Freestream reference collector.

Papadakis[2] for both the water and air injection systems. The system of Papadakis was modified for these tests such that the air and water solenoids were controlled by a computer data acquisition system.

The model constructed for these tests was a four-bladed propeller which was mounted on a special test stand in the wind tunnel. Each of the four blades of the propeller were manufactured from a single mold and were based on a constant chord, Clark-Y airfoil section. The propeller blades further incorporated a twist of 2.75°/inch. Fully assembled the propeller used had a diameter of 3 feet and was typically rotated at a constant speed of 500 RPM. The complete model, as tested, is shown in Fig. 3.

In order to determine the freestream LWC values for the calculation of β, a reference collector was assembled. The freestream reference collector used contained four, 20-inch collectors which were mounted perpendicular to the airflow and $^1/_2$ a propeller diameter in front of the nacelle. The reference collector was rotated during testing to provide an average value for the freestream reference value at each radial location. The freestream reference collector is illustrated in Fig. 4.

The water used in these tests was saturated with FD&C Blue Dye No. 2 to a concentration of 0.5 g/L of deionized water. The dye laden water was injected through the spray nozzles, using the spray system, at known air and water pressures for a given spray time. The pressures at the nozzles were monitored with two 0-250 psig pressure transducers on the water supply lines and a 0-100 psig transducer on the air line. The air and water on/off states were controlled by solenoid valves which were computer activated by a relay switch. Before testing the spray system was calibrated using a PDPA system[4]. The spray calibration results were used to determine the air and water pressures used in the propeller testing.

The dye laden water in the reultant spray cloud was then allowed to impinge for a given amount of time on both the model and reference collector which were coated with paper. In the original tests of von Glahn and Papadakis a blotter paper had been used to collect the dye on the models. In the current tests, a form of chromatography paper was used. It was determined that this paper formed to the model contour without the wrinkling which was found with the blotter paper. An added benefit of this paper was the high level of consistency in paper color, unlike the blotter paper which was composed of courser wood pulp.

For the propeller testing it was further found that the paper strips had to be protected on the inner radial side from run back. This was accomplished by placing a guard strip of paper on the inner radial side of each collector strip. The radial locations tested and the guard strips locations are illustrated in Fig. 5.

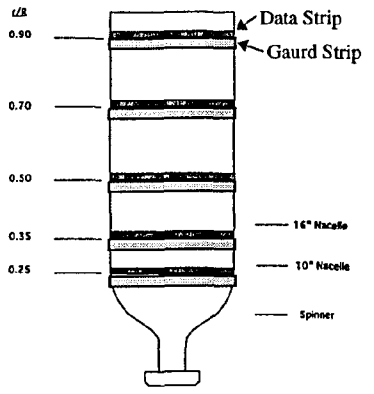

Figure 5. Main blotter strip locations tested.

After the dye deposition had been accomplished in the wind tunnel, the data strips were taken to NASA Lewis Research Center for digitization. Before discussing the specifics of the digitization a brief

Copyright ©1997, American Institute of Aeronautics and Astronautics, Inc.

discussion of the theory behind the method should be presented.

The main theoretical background for the digitization is that of diffuse-reflective spectroscopy and more specifically the theory of Kubelka and Munk[5]. The theory of Kubelka-Munk (KM) relates the transmittance and reflectance of monochromatic light off a plane-parallel layer composed of light-scattering and light-absorbing particles whose dimensions are much smaller than the layer thickness, i.e. the paper thickness. The Kubelka-Munk theory is the main theoretical background behind the chemical practice of thin-layer chromatography which determines chemical composition and quantities of samples of a material on chromatography paper. The Kubelka-Munk theory is really a set of ordinary differential equations which were solved by Kortüm[5] for the case of a thin layer of a substance on a backing paper. The equation for the reflectance and transmittance is therefore given by Eq. 3a and 3b, respectively.

$$R = \frac{1 - R_g[a - b \cdot \coth(b \cdot S \cdot X)]}{a + b \cdot \coth(b \cdot S \cdot X)} \qquad (3a)$$

$$T = \frac{b}{a \cdot \sinh(b \cdot S \cdot X) + b \cdot \cosh(b \cdot S \cdot X)} \qquad (3b)$$

where:

$$a = \frac{S + K}{S}$$

$$b = \sqrt{a^2 - 1}$$

In the above equation R is the percent reflectance of the incident light (I/I_o), T is the normalized transmittance, S is the scattering coefficient of the dye in this case, X is the thickness of the dye layer, and R_g is the reflectance of the backing paper.

In the practice of thin-layer chromatography it is frequently assumed that the thickness of the dye layer is infinite from a optical point of view. Assuming that, for the moment, that the layer is infinitely thick then the Kubelka-Munk remission function can be used as expressed in Eq. 4. In this equation, K is the absorptivity coefficient of the dye layer.

$$\frac{K}{S} = \frac{(1 - R_\infty)^2}{2 \cdot R_\infty} \qquad (4)$$

It was found by Huf[6] that a layer could be considered infinitely thick from an optical point of view when the quantity b·S·X was greater than 2. For the dyes used in these experiments this was the case, based upon an analysis of Papadakis[2] data.

In order to use the analysis technique of either laser reflectance or digital imaging the dye must not be allowed to soak into the paper beyond the upper layer of the paper. If the dye is assumed to be a transparent layer on a totally reflecting substrate, i.e. the undyed paper, and, using the undyed paper as a reference (100% reflectance of the incident light), it can be assumed that the Kubelka-Munk remission function can be applied as follows[7]:

$$KM(I_{nc}) = \frac{(1 - I_{nc})^2}{2 \cdot I_{nc}} = \frac{\varepsilon \cdot c(I_{nc})}{S} \qquad (5)$$

Equation 5 relates the normalized intensity ($I_{nc} = R$), the molar absorption coefficient (ε), the concentration of dye (c), and the scattering coefficient (S). If it is further assumed that the scattering coefficient of the dye layer was constant, the equation for the concentration is:

$$c(I_{nc}) = \frac{S \cdot KM(I_{nc})}{\varepsilon} = B \cdot KM(I_{nc}) \qquad (6)$$

The interesting thing about this equation is that B is a constant which will depend only on the choice of dye and paper. The concentration, c, of a substance is related to the mass of the substance by the following relationship:

$$\frac{\text{mass}}{\text{unit area}} = c \cdot X = \frac{K \cdot X}{\varepsilon} \qquad (7)$$

In order to determine the dye concentration, based upon the normalized reflected light intensity, a calibration would then be required in a manner similar to that used to determine the dye mass by von Glahn[1].

The definition of β is the mass flux of water impinging on a surface non-dimensionalized by the mass flux of water in the freestream. In the experiment the definition of β was defined as the mass of water which impinged on the model over a given time non-dimensionalized by the mass of water which was deposited on the reference collector for the same length of time. Because the dye concentration was held constant throughout the tests, the equation for β can be expressed as the mass of dye deposited on the paper non-dimensionalized by the dye deposited on the freestream collector, Eq. 8. In this equation a correction factor, E_{fs}, was applied to account for the collection efficiency of the freestream collector.

Copyright ©1997, American Institute of Aeronautics and Astronautics, Inc.

$$\beta = \frac{(mass\ of\ dye)_{propeller}}{\frac{1}{E_{fs}} \cdot (mass\ of\ dye)_{freestream\ collector}} = E_{fs} \cdot \frac{B \cdot KM}{B \cdot KM_{fs}} \quad (8)$$

In Equation 8 the quantity B is a constant which can be cancelled. Now, the equation for β is given by Eq. 9.

$$\beta = E_{fs} \cdot KM/KM_{fs} \quad (9)$$

The data reduction procedure was, therefore, reduced by eliminating the need to determine the constant required for the dye mass determination, Eq. 6. This relationship was found to hold for airfoil data strips which were tested previously[3] and the relationship was used in the propeller testing.

Digital Imaging Procedure

The freestream and model data strips were all imaged at the NASA Lewis Research Center using a 14-bit, liquid-cooled, CCD-array camera. As shown in Fig. 6 the dye-laden strips were placed under a photographic grade non-reflective glass, next to a scale (to provide a reference length) and illuminated by two light sources. The light sources used were air cooled halogen bulbs. The light from the halogen bulbs was filtered through a yellow band pass filter around 600 nm ± 25 nm and passed through a diffusion filter to reduce the peak light levels. Before digitization, care was taken to produce the most uniform lighting possible in order to reduce the correction factor for light intensity variations. The resulting light reflected from the dye-laden paper was then imaged by the digital camera through a 412 - 525 nm band pass filter in order to increase the pixel sensitivity in the blue region and decrease the absorption of extraneous light. The camera took images consisting of a 512 by 512 pixel array, each pixel resolved in intensity to 14 bits. Each final image was an average of 8 separately acquired images with the black image subtracted. The digitized image was then stored for later analysis. An example of image taken during the tests is shown in Fig. 7. Notice in this image that several strips were recorded at the same time, lined up by the leading edge marks, and that each image included a length scale and color reference.

After collecting all of the images, a flatfield image was created using the camera, the lens, the filters, the lights and a light integrating sphere. This flatfield image set, which consists of a dark image (I_D), a bias image, and a flatfield image (I_{FF}), is later applied in the image analysis routines to reduce the non-uniformity in pixel response across the CCD array. In order to correct the

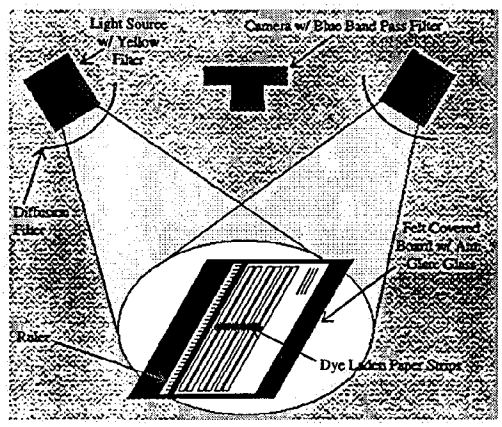

Fig. 6. Digitization setup.

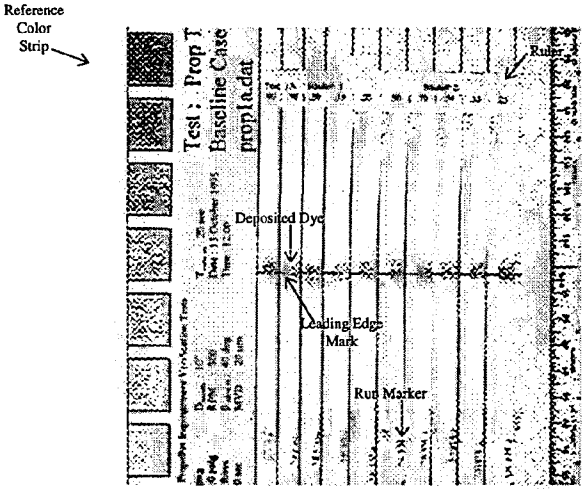

Figure 7. Example image acquired of data strips.

intensity, I, of an image the flatfield images were applied to the intensity of each pixel of the image by use of the Eq. 10 in order to arrive at a new flatfield corrected image, I_{FFC}.

$$I_{FFC} = \frac{I - I_D}{I_{FF} - I_D} * Avg(I_{FF} - I_D) \quad (10)$$

The flatfield correction corrected for variation in the camera response due to angularity of light with the spherical lens and also corrected for pixel-to-pixel sensitivity in the CCD array to light levels.

The digitized images were processed using a software package called PV-Wave™, with specially developed processes (programs) to manipulate the images. Each digitized image was read into PV-Wave™, along with the white reference and flatfield

Copyright ©1997, American Institute of Aeronautics and Astronautics, Inc.

images, and the length scale was then defined automatically using the digitized scale, which typically yielded 0.3 mm per pixel. The user was then prompted to enter two points which defined a box around the area to be interrogated. The leading edge of each strip was marked at the time of the tests and the program automatically determined this location by interrogation of the image. After the leading-edge location was determined, and the user entered the interrogation limits, the program iterated from the user specified upper surface s/c location to the user specified lower surface s/c location determining the left and right edges of the paper at each location using a gradient approach. At each s/c location the pixels from the left to right edges of the strip were then averaged for a single value. At this point in the reduction process, a 1-D array of light intensity values versus surface distance on the model existed.

Some non-uniformity of the incident lighting at the time of digitization was unavoidable, and led to a non-uniformity in the reflected light. This non-uniformity was corrected by normalizing (dividing) the entire image by the reference "white" image, which included the same non-uniformity, for every pixel in the image This yielded the normalized intensity I_n given by:

$$I_n(S) = I(S)/I_{wr}(S) \qquad (11)$$

Numerically this was implemented by averaging a group of pixels in the white reference image centered on the same pixel locations as the row on the strip being analyzed. This value was then used as the $I_{wr}(S)$ value in Eq. 11. The normalization effectively reduces the effects of non-uniformity in the lighting at the time of the digitization.

After normalization the image was further corrected for any changes in the image due to slight variations in the mean incident light intensity. This was accomplished by using the white (non-dye-laden) region on either end of the strip being reduced to determine a correction factor. The correction factor, the white pixel intensity from the reference image taken at the corresponding location, $I_{wr}(S_{end})$, divided by the intensity of the above white region, $I(S_{end})$, was then multiplied by the normalized intensity. Then the normalized corrected intensity becomes:

$$I_{nc}(S) = \left(\frac{I(S)}{I_{wr}(S)}\right)\left(\frac{I_{wr}(S_{end})}{I(S_{end})}\right) \qquad (12)$$

With normalization and the correction factor applied, values of normalized corrected intensity, I_{nc}, of 1.0 were found at the end of each strip, where no dye is present, and values less than one between the limits of impingement where dye was present. The minimum normalized corrected intensity occurred where the dye concentration was a maximum.

Using the Kubelka-Munk remission function the normalized, corrected light intensities were then transformed into a new variable, KM. The freestream value of the Kubelka-Munk variable, KM_{FS}, was determined by a similar data reduction process on the reference collector blotter strips. Using all of the above, $\beta(S)$ was then given by Eq. 9. All valid cases were then averaged to form a single beta curve. Typically 12 data strips were averaged for a single curve.

The collection efficiency of the freestream reference collector, E_{rc}, was determined using the numerical results of Lewis and Brun[8]. Lewis and Brun numerically determined the collection efficiency of rectangular bodies and used the results to determine an equation for the collection efficiency.

Uncertainty Analysis

An uncertainty analysis has been performed on the propeller droplet impingement experiment for the purpose of identifying the parts of the experiment where a reduction in uncertainty will most improve the accuracy of the final propeller droplet impingement data. The analysis will ultimately provide an estimate of the uncertainty in the final data to facilitate its use for computer code validation. An analysis of the uncertainty in the airfoil droplet impingement data has previously been published in Ref. 3. The analysis presented here is based on the work of Kline and McClintock[9] and the more recent work of Coleman and Steele[10] where the uncertainty estimate means that the odds are 20 to 1 that a single sample will lie within ± the uncertainty estimate from the true value.

Using the dye tracer method of droplet impingement, the equation for β was given by Eq. 13 where the variables are defined below. Using Eq. 13, the uncertainty of β can be estimated by Eq. 14. The uncertainty in all three of these quantities must be determined.

$$\beta = \frac{\overline{m}_d(s,r)}{\overline{m}_{d_{fs}}(r)} E_{rc}(r) \qquad (13)$$

$\overline{m}_d(s, r)$ mass of dye deposited on a propeller strip per unit area

$\overline{m}_{d_{fs}}(s, r)$ mass of dye deposited on reference collector strip per unit area

E_{rc} Collection efficiency of the reference collector

Copyright ©1997, American Institute of Aeronautics and Astronautics, Inc.

s surface location in chordwise direction on the propeller strip

r radial location on the propeller strip

$$\frac{w_\beta}{\beta} = \pm\sqrt{\left(\frac{w_{\bar{m}_d}}{\bar{m}_d}\right)^2 + \left(\frac{w_{\bar{m}_{d\,fs}}}{\bar{m}_{d\,fs}}\right)^2 + \left(\frac{w_{E_{rc}}}{E_{rc}}\right)^2} \qquad (14)$$

Uncertainty in the mass in the freestream and propeller dye mass at any location will be dependent upon the uncertainty in several different quantities: the propeller speed, the radial location of measurement, the test section velocity, the LWC and MVD of the spray cloud, the timing, the blade setting, the concentration of the dye, the errors in the camera, and the freestream turbulence. The last uncertainty, due to freestream turbulence, was initially neglected in the uncertainty analysis.

Neglecting the freestream turbulence term at this point, the uncertainties, w_{md}/m_d, in the mass of dye deposited on the propeller and freestream reference collector were determined to be ± 2.4% for a 20 micron MVD spray cloud at the 70% radial location. The uncertainty in the reference collector efficiency at the same location and conditions was determined to be ± 2.9%. Combining the uncertainties listed above, the uncertainty in the impingement efficiency, for the 20 μm MVD spray cloud, was found to be ±4.42% over the entire propeller.

The calculated uncertainty for this case is much less than the values determined by Papadakis, et al.[2], of 10-25% or Bragg, et al.[3], of 15.44%. Several different factors worked together to make the magnitude of the uncertainty found in this analysis so low. One factor which has been neglected is the error in the reference collector efficiency, E_{rc}, as a function of the radius for the rotating collector used in the testing. Until computational methods exist to predict the collection efficiency for this rotational case, the 2-D, non rotating, values determined using the formulas of Lewis and Brun[8] have been used in the reduction.

The other major omission in this error analysis has been the unsteadiness of the freestream due to tunnel turbulence and spray cloud unsteadiness. There is no simple way to calculate this uncertainty a priori. Bragg, et al.[3], dealt with this uncertainty by taking twice the standard deviation of the freestream dye mass, as measured on the reference collector, to obtain a 95% confidence level (20:1 odds) for the uncertainty. Using this approach, the uncertainty in the propeller tests, as a function of the radial location, was determined from the freestream reference collector data. It was found that the twice the standard deviation of the dye mass on the freestream reference collector was between 3%-14.4%. Based upon the factors previously analyzed the expected uncertainty in the dye mass on the freestream reference collector was at most 1.5%-3%. The freestream turbulence and spray cloud unsteadiness, based upon the comparison of the test data and the uncertainty analysis presented in this chapter, dominates the uncertainty of the droplet impingement tests. Based upon this difference in uncertainty, between the derived and experimental values, the impingement testing has the possibility of being very accurate if the freestream turbulence in the spray cloud could be made more uniform and repeatable.

The deviation in the mass of dye collected on the freestream collector, the standard deviation in the propeller data at each radial location, and the collector efficiency at each radial location were used to calculate the uncertainty in the impingement efficiency, w_β/β. Figures 9 summarizes these data for the 20 μm MVD spray cloud using the data of the baseline geometry propeller tests. In this figure the uncertainty is presented as the percentage of w_β/β. Notice that at the s/c = 0.0 - 0.01 location, which correspond to the locations of β_{max}, has the minimum uncertainty levels, w_β/β, of 8%-16%. In Figure 9 also notice that the uncertainty in β increased as the impingement limits were approached. The increase in uncertainty at the outer edges of Fig. 9 correspond to the locations where β approached zero. At the impingement limits a slight uncertainty in β will result in a large percentage uncertainty. The uncertainty in the impingement efficiencies shown in Fig. 9 provide further illustration that the derived uncertainty of approximately 4% for the 20 MVD case was optimistic. Based upon the experimental data the uncertainty in the impingement efficiency in these tests was therefore less than or equal to 16% at β_{max} and increased as the impingement limits were approached to 30%-50%.

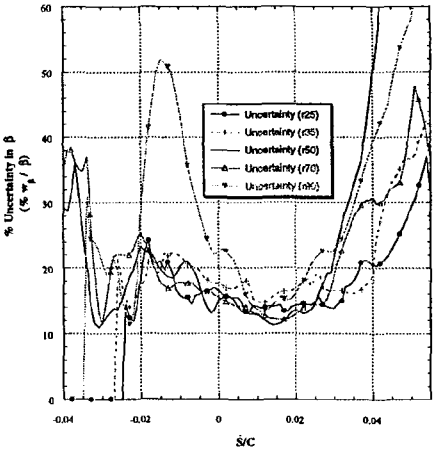

Figure 9. Uncertainty in 20 μm MVD data

Copyright ©1997, American Institute of Aeronautics and Astronautics, Inc.

RESULTS AND DISCUSSION

The baseline propeller was a four-bladed configuration with $\beta_{0.75R}$ = 40° and a 10"-diameter, axisymmetric nacelle. The first propeller impingement experiments used a 20 μm MVD spray cloud and the results are included in Fig. 11. Figure 11 presents the experimentally determined impingement efficiency (β) as a function of the radial and chordwise location.

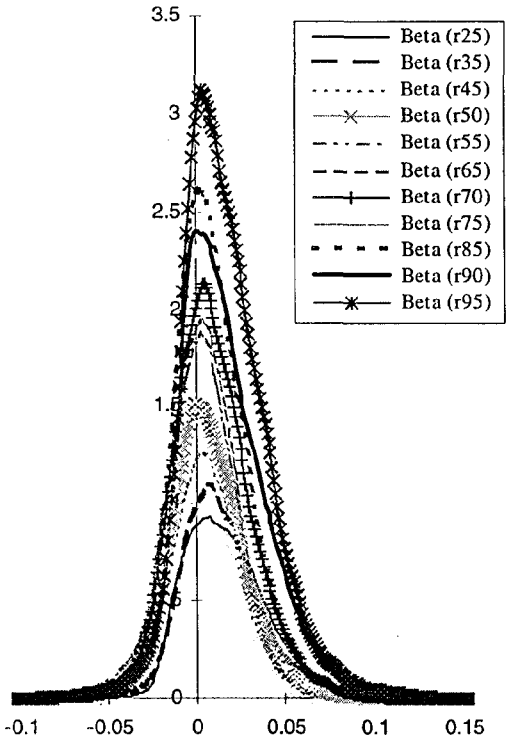

Figure 10. 20 μm MVD data.

The values of β, in Fig. 10, were found to vary with both radial location and chordwise, S/C, location. Maximum values of β were found to occur for this baseline case at S/C locations of approximately 0.005. As the radial location of the measurement was moved outward from r/R = 0.25 to 0.95, the maximum value of the impingement parameter, β_{max}, varied from 0.93 to 3.12, Fig. 10.

In general the lower surface impingement moved toward the stagnation line on the propeller (S/C ≈ 0.0 - 0.01 for the current geometry and conditions), when the radial location analyzed was varied between 0.25 and approximately 0.70 - 0.75. When the radial location of measurement was increased further the lower surface impingement limits were found to move outward again. On the upper surface, the impingement limits were again moved towards the stagnation line as the radial location analyzed was increased but, for the upper surface past the r/R = 0.50 location, the upper surface impingement limits were found to move away from the stagnation line of the propeller.

The variation in the impingement limits is partially explained by the variation in the lift coefficient with radial location. Figure 11 shows the predicted distribution of C_ℓ using a three-dimensional panel code for a propeller, BetaProp[11], and a two-dimensional strip theory. Both methods show that the sectional lift coefficient increased with radial extent on the blade up to the 0.55-0.65% radial location. The sectional lift coefficient of the blade was directly proportional to the sectional angle of attack of the propeller blade at each radial location. Increasing the angle of attack on an airfoil will move the lower surface impingement limits farther aft while the upper surface impingement limit will be moved toward the stagnation point. The impingement limits of the baseline propeller data, Fig. 11, follows the trends which would be expected based upon the predicted variation in the sectional C_ℓ values.

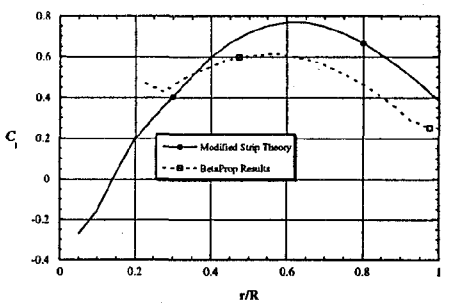

Figure 11. Variation in C_ℓ for propeller.

Notice in Fig. 10 that the maximum impingement efficiencies for the baseline data were greater than unity for the majority of the radial locations. In typical impingement calculations, i.e. for non-rotating structures, values of β greater than one are not usually found. β was defined as the mass flux striking a surface non-dimensionalized by the freestream value. The freestream mass flux was based upon the freestream velocity, while each location on the propeller sees an effectively larger approach velocity based upon the additional angular velocity due to the rotation of the propeller. Therefore, the propeller, as the radial distance was increased, swept out more water in the spray cloud and its impingement increased. Since β was based upon the freestream value, β increased in the radial direction and significantly exceeded one for the majority of the baseline data, Fig. 10.

Copyright ©1997, American Institute of Aeronautics and Astronautics, Inc.

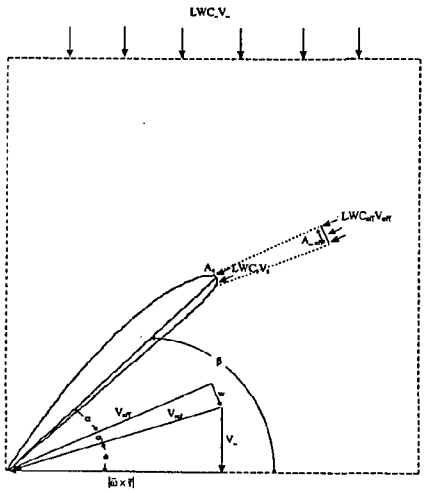

Figure 12. Illustration of control volume used.

The trend of an increase in β as the radial location is increased can be mathematically related to the impingement on an airfoil using blade element theories. Figure 12 illustrates the reference frame and variables used for the derivation of the three-dimensional value of β from the two-dimensional blade element theory. Figure 12 presents a slice of the propeller blade surrounded by a control volume which was the fixed frame of reference for the following derivation. In this figure, the air approaches the blade element from right to left due to the rotation of the propeller and through the top of the control volume due to the freestream velocity. In order to simplify the equations, the effects of the inflow (w) were ignored. In this analysis, in a manner consistent with the derivation of airfoil impingement codes, the freestream mass which impinges on the model is assumed to start an infinite distance from the propeller. For the derivation presented, all of the mass which impinges on the propeller was assumed to pass through the area $A_{\infty\,eff}$ which is perpendicular to the effective velocity, V_{eff}, of each propeller section. In this frame of reference the equation for the conservation of mass becomes:

$$LWC_{eff}V_{eff}A_{\infty eff} = LWC_sV_sA_s \qquad (15)$$

Where the subscript $(\,)_{eff}$ quantities represent the effective values of the various quantities which would pass through the area $A_{\infty\,eff}$ if the airfoil segment, as assumed in blade element theory, were stationary and fixed at the effective angle of attack, α. In this frame of reference the definition of the impingement efficiency would be:

$$\beta_{2-D} = \frac{LWC_sV_s}{LWC_{eff}V_{eff}} = \frac{A_{\infty_{eff}}}{A_s} \qquad (16)$$

The three-dimensional impingement efficiency is non-dimensionalized by the freestream mass flux, and not the effective values, as shown in Eq. 17.

$$\beta_{3-D} = \frac{LWC_sV_s}{LWC_\infty V_\infty} \qquad (17)$$

Combination of Eq. 16 and 17 yields:

$$\beta_{3-D} = \beta_{2-D}\frac{LWC_{eff}V_{eff}}{LWC_\infty V_\infty} \qquad (18)$$

Now, in order to simplify the analysis, the concentration of water (frequently called the liquid water content, LWC) in the freestream, LWC_∞, is assumed equal to the LWC at the effective area of the 2-D slice from the blade element theory. The water concentration is not a vector quantity and, therefore, the assumption of equality between the effective water concentration and the water concentration in the freestream will be valid unless significant levels of propeller stream tube contraction occur. This contraction will later be included, but was ignored at this point such that Eq. 18 becomes:

$$\beta_{3-D} = \beta_{2-D}\frac{V_{eff}}{V_\infty} \qquad (19)$$

If it is further assumed that the induced velocity, w, was negligible then, from Fig. 12, the effective velocity at the propeller location was:

$$V_{eff} = \left[V_\infty^2 + \omega^2 r^2\right]^{1/2} \qquad (20)$$

Using Eq. 20 in Eq. 19 it can be found that:

$$\beta_{3-D} = \beta_{2-D}\frac{\left[V_\infty^2 + \omega^2 r^2\right]^{1/2}}{V_\infty} \qquad (21)$$

Simplifying Eq. 21 it was found that:

$$\beta_{3-D} = \beta_{2-D}\left[1 + \frac{\omega^2 r^2}{V_\infty^2}\right]^{1/2} \qquad (22)$$

Based upon this simplified approach for the derivation of the impingement efficiency, and assuming

Copyright ©1997, American Institute of Aeronautics and Astronautics, Inc.

the maximum two-dimensional impingement efficiency, as typically assumed, was one, then the propeller impingement efficiency, $\beta_{3\text{-}D}$, can exceed one if ω is greater than zero. Therefore, as the radial location of the impingement measurement on the propeller increased, the maximum impingement efficiency, β_{max}, increased, in a manner consistent with the test data, Fig. 11.

An example of using this idea with Bragg's AIRDROP[12] code is shown in Fig. 13 for the baseline propeller case. In order to determine the data of Fig. 13, the propeller was modeled using the same modified strip theory analysis that was used to design the propeller. From this analysis the C_ℓ values for the radial locations of interest were obtained. The C_ℓ values were then matched with the 2-D airfoil flowfield results to determine the effective airfoil angle of attack as a function of radial location on the propeller. The droplet inertia parameter and Reynolds number were calculated using the airfoil chord as the characteristic length and the effective velocity as the characteristic velocity. Using this angle of attack, the inertia parameter and Reynolds number were calculated and input into the 2-D droplet impingement code for the radial locations of interest. In order to compute the 3-D impingement values which corresponded to the propeller cases, the 2-D β values were then multiplied by the velocity ratio derived previously, Eq. 22.

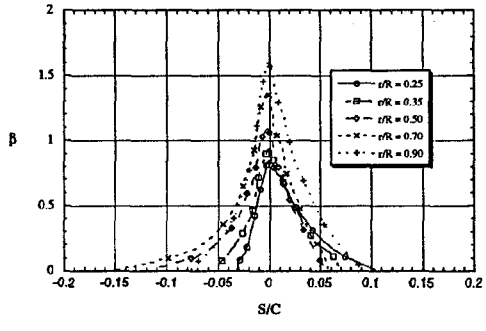

Figure 13. 2-D determined β values.

The 2-D calculated β_{max} appropriately increased, Fig. 13, as the radial location analyzed was increased, but the theoretical values were lower in magnitude than the experimentally determined values, Fig. 10. The limits of impingement on the upper surface were predicted reasonably well by the 2-D strip theory approach, Fig. 13, when compared to the experimental data, Fig. 10. However, on the lower surface, the experimentally determined increase in S_L with increasing radial location was predicted, but the magnitude of the change was greatly over predicted by the theory. Overall, however, the 2-D method and the experimental data agree for this case with regards to the impingement limits.

In the above derivation the influence of the other propeller blades, the propeller thrust (and therefore the inflow), and the contraction of the stream tube have been neglected. These quantities are all likely to increase the water concentration near the propeller which was previously assumed equal to the freestream value. If now the effective water concentration near the propeller were allowed to vary from the freestream value, then Eq. 22 must be rewritten as shown in Eq. 23.

$$\beta_{3-D} = \beta_{2-D}\left(\frac{LWC_{eff}}{LWC_\infty}\right)\left[1+\frac{\omega^2 r^2}{V_\infty^2}\right]^{1/2} \qquad (23)$$

For the actual propeller run in this report, thrust was produced and the area of the stream tube of air which passed through the propeller was contracted from a larger area in the freestream. The contraction of the airflow stream tube will increase the water concentration near the propeller, LWC_{eff}. As the thrust, and therefore, the stream tube contraction increase, the maximum impingement efficiency will increase. The increase in the levels of β with increasing thrust can be found in the engine nacelle impingement data of Papadakis[2]. In addition to the stream tube contraction due to the thrust, the spinner and nacelle will further alter the effective LWC seen by the propeller and increase β based upon Eq. 24. Based on all of these factors, the 3-D impingement measured on the propeller should be larger than the values predicted by the two-dimensional strip analysis.

All of the data presented in this report are preliminary. Later analysis of the data revealed that the data at the outer radial locations, r/R > 0.50, may contain an error in the freestream measurements. This issue is still being pursued at this time.

SUMMARY AND CONCLUSIONS

The digital imaging and image analysis data reduction scheme presented in this report offers a significant savings in both time and expense over current methods. This method was used to study the impingement efficiency on a propeller. The propeller impingement testing was the first of its kind and therefore needs to be analyzed in more detail before the confidence in the data can be increased. The propeller tests illustrated that for rotating systems the impingement efficiency can be greater than one, a fact that was explained using blade element theory.

Copyright ©1997, American Institute of Aeronautics and Astronautics, Inc.

RECOMMENDATIONS

The following recommendations are suggested in order to further improve droplet impingement testing:

1. Reduce the turbulence level and, therefore, the spray cloud unsteadiness in the wind tunnel if mixing can be maintained.
2. The linear relationship between the dye mass and the KM variable needs further verification.
3. A light box should be used for the imaging operations to eliminate outside light interference
4. The freestream reference collector needs to be improved for both propeller and airfoil testing.
5. A large number of repeat runs are suggested to reduce the statistical uncertainty of the data.

ACKNOWLEDGEMENTS

The authors would like to thank the following individuals and organizations for supporting this research: Michael Cebryznski who aided in taking all of the wind tunnel data, Abdi Khodadoust who performed the airfoil verification tests, NASA Lewis and Tim Bencic for the use of the digital camera and spray system, BFGoodrich Aerospace for funding this research, and all of the graduate and undergraduate students whose long hours helped see this project through.

REFERENCES

[1] von Glahn, U. H., Gelder, T. F., and Smyers, W. H., Jr., *A Dye Tracer Technique for Experimentally Obtaining Impingement Characteristics of Arbitrary Bodies and a Method for Determining Droplet Size Distributions,* NACA TN 3338, March 1955.

[2] Papadakis, M., Elangonan, R., Freund, G. A., Jr., Zumwalt, G. W., and Whitmer, L., *An Experimental Method for Measuring Water Droplet Impingement Efficiency on Two- and Three-Dimensional Bodies,* NASA CR 4257 (DOT/FAA/CT-87/22), Nov. 1989.

[3] Bragg, M. B., Cebrzynski, M., Reichhold, J. D., Sweet, D., Waples, T., and Shick, R., "An Experimental Method for Water Droplet Impingement Measurement", 1995 American Helicopter Society/Society of Automotive Engineers International Icing Symposium, Montreal, Canada, Sept. 18-21, 1995.

[4] Reichhold, J. D., "Experimental Determination of the Droplet Impingement on a Propeller Using a Modified Dye-Tracer Technique", M.S. Thesis, University of Illinois at Urbana/Champaign, Urbana, IL, Jan. 1997.

[5] Kortüm, G., *Reflexions Spectroscopie,* Springer-Verlag, Berlin, 1969.

[6] Huf, F. A., Anal. Chim., Acta 90, p. 143, 1977.

[7] Huf, F. A., "In Situ Evaluation of Thin-Layer Chromatograms," *Quantitative Thin-Layer Chromatography and Its Industrial Applications,* editor Laszlo R. Treiber, Chromatographic Science Series, Vol. 36, Marcel Dekker, Inc. New York, pp. 17-66, 1987.

[8] Lewis, William and Brun, Rinaldo J., "Impingement of Water Droplets on a Rectangular Half Body in a Two-Dimensional Incompressible Flow", NACA TN 3658, 1956.

[9] Kline, S.J. and McClintock, F.A., "Describing Uncertainties in Single Sample Experiments", *Mechanical Engineering,* Vol. 75, pp. 3-8, Jan. 1953.

[10] Coleman, H.W. and Steele, W.G., *Experimentation and Uncertainty Analysis for Engineers,* John Wiley and Sons, Inc., New York, 1989.

[11] Farag, K. Private Communication, January 1996.

[12] Bragg, M. B., "Rime Ice Accretion and Its Effects on Airfoil Performance," Ph.D. Dissertation, The Ohio State University, Columbus, OH, 1981, and NASA CR 165599, March 1982.

Copyright ©1997, American Institute of Aeronautics and Astronautics, Inc.

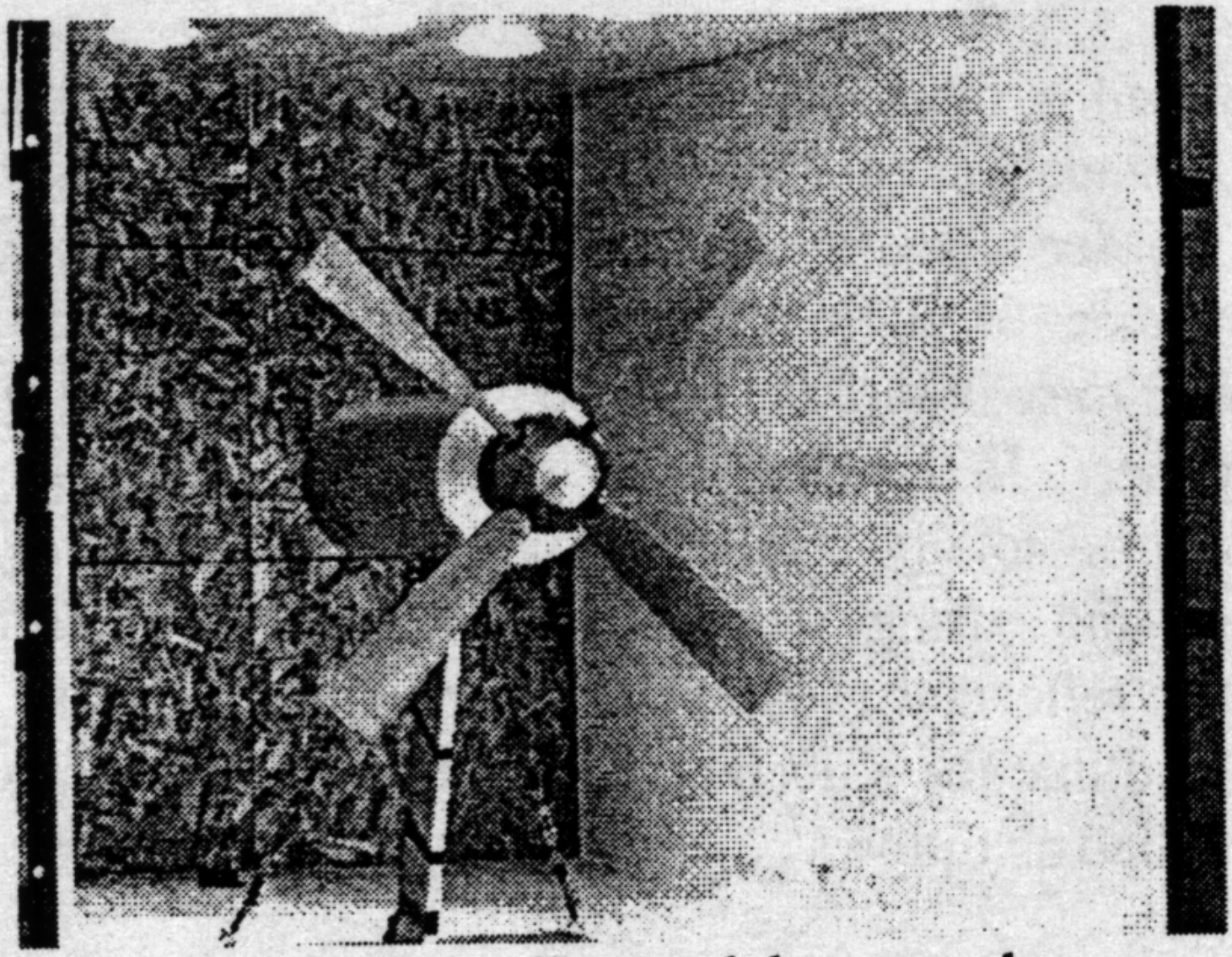

Fig. 3. Propeller model as tested.

Copyright ©1997, American Institute of Aeronautics and Astronautics, Inc.

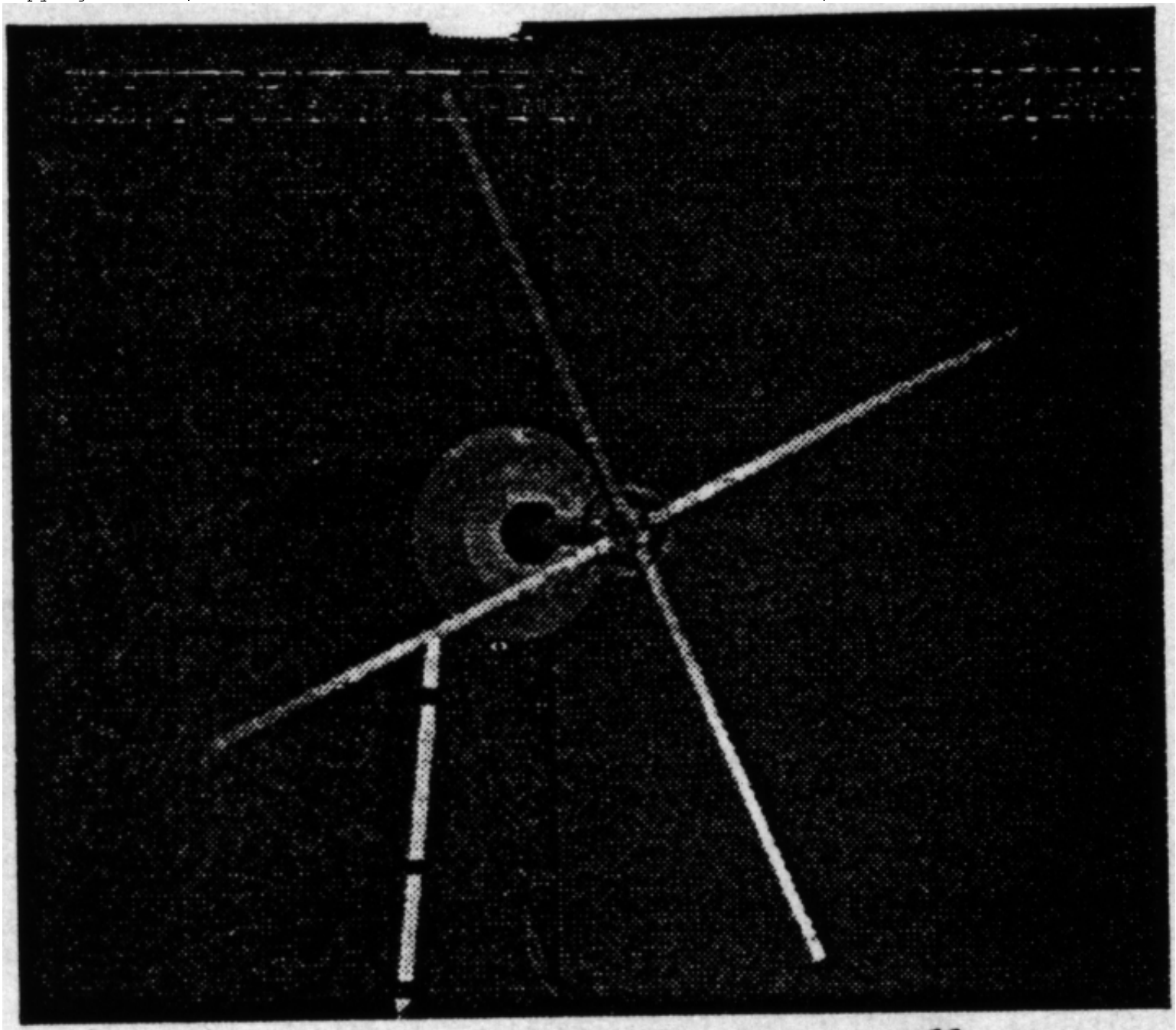

Fig. 4. Freestream reference collector.